Publ. Astron. Obs. Belgrade No. 98 (2018), 59 - 68 *Invited Lecture*

SHOCK WAVES IN INTERSTELLAR GAS AND THE SOLAR CORONA

J. C. RAYMOND

Harvard-Smithsonian Center for Astrophysics, 60 Garden St., Cambridge, MA 02138, USA
E–mail: jraymond@cfa.harvard.edu.

Abstract. A shock wave is a sharp transition from supersonic to subsonic flow in a narrow interval. The shock transition in neutral gas occurs by means of collisions, and those collisions bring the gas to a new thermodynamic equilibrium. Shocks in plasmas are governed by electromagnetic fields and plasma turbulence, and they do not generally lead to thermal equilibrium. Electron, proton and ion temperatures can be very different, and the shocks can produce non-thermal velocity distributions, including cosmic rays or solar energetic particles. This paper will review observations of shocks in supernova remnants and the solar corona that indicate those non-equilibrium conditions.

1. INTRODUCTION

Shock waves in the Earth's atmosphere and in most textbooks are collisional. That is, they are jumps in the fluid velocity, density and temperature that occur over a narrow layer whose thickness is approximately the collisional mean free path. For most purposes, they are simply described by the Rankine-Hugoniot jump conditions, which give the changes in speed, density and temperature as functions of the ratio of shock speed to pre-shock sound speed, known as the Mach number, M. In the high Mach number limit, a strong shock compresses the gas by a factor of 4. The post-shock temperature of a strong shock depends on the mean mass of the particles, and for an ionized gas of typical astrophysical abundances it is about $1.4 \times 10^5\ V_{100}^2$ Kelvin, where V_{100} is the shock speed in units of 100 km/s. If the magnetic field strength is significant, these relations are modified to the magnetohydrodynamics jump conditions. Draine & McKee (1993) review astrophysical shocks.

While a collisional shock by definition is mediated by collisions and therefore maximizes entropy by establishing thermal equilibrium, the shocks in most astrophysical plasmas are collisionless. That is, the shock jump occurs by way of interactions between the particles and electromagnetic fields or turbulence over a scale comparable to the proton gyroradius or the ion skin depth, $\omega_{\rm pi}/c$, where $\omega_{\rm pi}$ is the ion plasma frequency and c is the speed of light. For typical ISM conditions of 1 cm^{-3} and 3 μG, the collisional mean free path is on the order of 3×10^{14} cm, while the collisionless shock thickness is around 10^8 to 10^9 cm.

A collisionless shock should still satisfy the Rankine-Hugoniot jump conditions, since those simply express conservation of mass, momentum and energy fluxes plus

the perfect gas equation of state. However, there is no reason to expect thermal equilibrium in the sense of equal temperatures of different species, or even in the sense of Maxwellian velocity distributions. For example, a collisionless shock might thermalize a fraction (1-1/X) of the bulk velocity of each particle species entering the shock, where X is the shock compression ratio. Then, if there is no exchange of energy among the species, each species would have a thermal energy and temperature proportional to its mass, $T_\alpha = m_\alpha/m_{\rm p}\ \ T_{\rm p}$. Moreover, supernova remnant shocks produce non-thermal emission detected in the radio, X-ray and gamma-ray bands, indicating extreme departures from Maxwellian distributions at high energies. These power-law tails in velocity account for cosmic rays (CRs) and the synchrotron emission at the boundaries of supernova remnants (SNRs) seen in the radio and in some cases in X-rays. Shock waves in the solar corona and solar wind also accelerate particles, solar energetic particles, or SEPs, though not to such high energies. The acceleration is generally explained by diffusive shock acceleration (DSA), in which particles scatter between the shock and a precursor region of plasma turbulence, gaining energy with successive scattering events.

It is important to understand collisionless shocks for several reasons. These shocks seem to generate cosmic rays at least up to around 10^{14} or 10^{15} eV in SNRs, and the SEPs produced by shocks driven by coronal mass ejections (CMEs) can affect satellites and astronauts. These shocks produce radiation that affects the evolution and heating of the ambient plasma. And finally, it is necessary to understand how observable diagnostics are related to shock parameters to correctly diagnose shock conditions in order to understand the basic energetics and evolution of the events that drive the shocks.

One important distinction for the discussion that follows is between radiative and non-radiative shocks. A radiative shock converts some fraction of the flow kinetic energy into thermal energy. The gas then radiates that energy away, returning to roughly the initial temperature. Because the radiation is usually generated by electron-ion collisions, it occurs over a collisional scale, and the plasma is able to approach thermal equilibrium. Therefore, most signatures of the physical processes at the shock are erased, and the emission spectrum is dominated by the bright emission generated far downstream.

On the other hand, a non-radiative shock is one in which the radiative cooling time is long compared to the important dynamical time scales such as the supernova remnant age. In that case, radiative cooling does not affect the dynamics, and radiation from far downstream does not dominate the spectra. In particular, H I Balmer lines and UV lines of He, C, N and O are produced in a narrow ionization zone just behind the shock front, so these lines carry the signatures of the plasma processes in the shock itself.

2. SHOCK DIAGNOSTICS

Very different diagnostics are available for investigating shocks in the solar wind, shocks in the ISM and shocks in the corona. The first can be studied *in situ*, while those in the ISM and corona are observed with remote sensing techniques.

Solar wind: Shocks in the solar wind can be detected by spacecraft carrying instruments that directly measure particle velocity distributions and electromagnetic fields. This has the enormous advantages that the observed quantities are not smeared out

over a range of shock conditions, that magnetic fields and plasma waves can be measured rather than inferred, and that complex non-Maxwellian velocity distributions can be measured in detail. Some limitations are that it can be difficult to determine the direction of the shock normal and that a single passage through a non-steady shock gives a snapshot that may be less useful than an average would be. Measurements by multiple spacecraft such as MMS can alleviate the difficulties, for instance in the study of whistler waves and non-thermal electrons (Oka et al. 2017). Another limitation is that shocks in the solar wind do not typically exceed Mach numbers of about 10, limiting the parameter space open to investigation. Measurements made *in situ* often have excellent time resolution, and they can cover a variety of particle species.

Solar Corona: Shocks in the solar corona have been observed for many years as type II radio bursts – bright emission in a narrow frequency range that drifts toward lower frequency as the shock propagates outward. A comprehensive review of solar radio emission is given by Pick & Vilmer (2008). Energetic electrons produced by the shock propagate through the plasma, forming an unstable bump-on-tail velocity distribution that can produce Langmuir waves at the electron plasma frequency, 9000 $n_e^{1/2}$ Hz. These waves, in turn, interact with low frequency waves or with other Langmuir waves to create radio waves at the plasma frequency or its harmonic, so the frequency gives the coronal density. Splitting of these bands has been interpreted in terms of the pre-shock and post-shock densities, which gives the shock compression. This can be combined with the shock speed and coronal density to estimate the coronal magnetic field (Vršnak et al. 2002; Mancuso et al. 2003).

Coronal shocks are also observed in white light with coronagraphs. With some modeling of the shape of the shock front, the intensity increase gives the compression (Ontiveros & Vourlidas 2009), and the standoff distance between the shock and the CME loops gives an estimate of the magnetic field strength (Gopalswamy & Yashiro 2011; Gopalswamy et al. 2012). The properties of the shock vary around its surface because both the shock speed and the strength of the perpendicular magnetic field change, so for instance the shock can have very different properties at the nose and on the flanks (Bemporad & Mancuso 2013; Susino, Bemporad & Mancuso 2015).

UV spectra of coronal shocks have been obtained with the UVCS instrument aboard the SOHO satellite (e.g. Raymond et al. 2000; Mancuso et al. 2002). The emission in the Lyα line dims, because H I atoms are accelerated and ionized, while Si XII emission brightens because of compression and ionization of lower silicon ions. O VI shows intermediate behavior, and its line width becomes larger as the kinetic temperature of oxygen increases. EUV images of coronal shocks have also been obtained with the AIA instrument aboard SDO. AIA bands corresponding to successively higher ionization states of iron brighten and dim as the iron is ionized, giving an estimate of the electron temperature (Ma et al. 2011).

Interstellar Medium: Non-radiative supernova remnant shocks are observed in the X-ray, optical and UV bands, though the optical and UV emission is rather faint. X-ray spectra give the electron temperature, and in some cases X-ray synchrotron emission reveals the population of non-thermal electrons. UV spectra give the line widths and kinetic temperatures of He, C, N and O. Shocks in partially neutral gas produce pure Balmer line optical filaments, and the two- or three-component profiles of the Hα line yield the proton kinetic temperatures, the post-shock electron

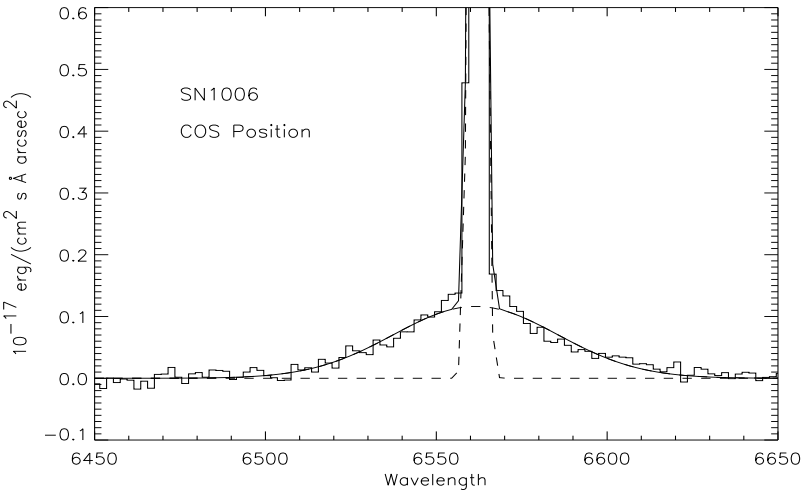

Figure 1: Two component profile of Hα from a 3000 km/s shock in SN1006 (Raymond et al. 2017). The narrow component is unresolved, while the broad component FWHM is 2600 km/s.

temperatures, and signatures of heating in shock precursors (Fig. 1). Radio and gamma-ray observations show high energy electrons and hadrons.

3. COLLISIONLESS SHOCK THEORY

A distinction is made between sub-critical and super-critical shocks. Sub-critical shocks are low Mach number shocks in which thermal conduction or viscosity can dissipate the energy in a smooth manner, while super-critical shocks rely on reflection of protons from the shock and streaming instabilities to produce plasma turbulence, and they are unstable. The critical Mach number depends on the angle between the magnetic field and the shock normal, and it can be up to 2.7. Treumann (2009) gives a comprehensive review of the physics of collisionless shocks.

Acceleration of cosmic rays and SEPs is a broadly important aspect of collisionless shock theory. It is a first order Fermi (1949) process in which particles are reflected from the shock itself and are scattered back to the shock by turbulence in a precursor region where streaming cosmic rays excite Alfvén waves or other modes. Blandford & Eichler (1987) review the analytic theory, which is known as Diffusive Shock Acceleration (DSA). The theory is appealing because a strong shock has a compression ratio of 4, and that gives a power law spectrum whose index is close to that measured in cosmic rays. An important question historically has been whether shocks that move parallel or perpendicular to the field accelerate particles more effectively. Quasi-perpendicular shocks accelerate particles quickly, but few particles are injected into the acceleration process, while the opposite is true for quasi-parallel shocks. Rippled shock structures or pre-shock fluctuations may combine the favorable aspects of both (Giacalone 2015).

Numerical investigations have extended the basic analytic theory. These include Monte Carlo and hybrid simulations that treat the protons as particles and the electrons as a neutralizing fluid (e.g. Ellison et al. 1996; Caprioli & Spitkovsky 2014). Particle-in-cell simulations treat both electrons and ions as particles, permitting self-consistent computation of the electromagnetic fields. (e.g. Sironi & Spitkovsky 2011). The results from kinetic models can be assimilated into analytic forms and then coupled with hydrodynamics codes to simulate SNRs (e.g. Slane et al. 2014).

4. ELECTRON-ION EQUILIBRATION

Early studies of shock waves assumed equal electron and ion temperatures behind shocks. Under that assumption electron temperatures, T_e, derived from X-ray spectra were used to determine shock speeds and study SNR evolution. More recently it has become apparent that electron-ion equilibrium is a good assumption for slow shocks, but the proton temperatures, T_p, are much higher than T_e in faster shocks.

In SNRs, this is seen in the Hα profiles of shocks in partially neutral gas. When hydrogen atoms and other neutrals pass through a collisionless shock they do not feel the effects of plasma turbulence or electromagnetic fields. Once they find themselves in the hot downstream plasma, they can be excited to produce Hα, they can be ionized, or they can undergo charge transfer reactions. Once they are ionized, they effectively become invisible. Those atoms that are excited before a charge transfer event produce Hα with a narrow velocity width corresponding to the pre-shock temperature, of order 10^4 K. On the other hand, roughly half the H atoms undergo charge transfer with post-shock protons, producing a population of H atoms with approximately the proton velocity distribution (Chevalier & Raymond 1978; Chevalier et al. 1980). Thus the proton temperature can be obtained from the width of the Hα broad component. The intensity ratio of the broad and narrow components depends on the relative rates of ionization and charge transfer, which in turn depends on T_e.

Ghavamian et al. (2001, 2002) used that method to show that T_e/T_p is about 1 in the 350 km/s shock in the Cygnus Loop, but only 0.4-0.5 in the $\sim$ 600 km/s shocks in RCW 86, less than 0.2 in Tycho's 2000 km/s shock and less than 0.07 in the 2500 km/s shock in SN1006. These trends are confirmed by comparing T_e determined X-ray spectra with the temperatures given by the Rankine-Hugoniot jump conditions and the shock speeds derived from proper motions and SNR distances for the Cygnus Loop (Medina et al. 2014) and SN1006 (Long et al. 2003).

In solar wind shocks, T_e and T_p can be measured directly, though there is considerable scatter in the ratio at any shock speed or Mach number. Schwartz (1988) found electron heating such that T_e/T_p is around 0.2 in solar wind shocks. More extensive measurements are presented in Ghavamian et al. (2013). They show a strong trend of T_e/T_p declining from close to 1 for very weak shocks to less than 0.1 for shock speeds above about 500 km/s or Mach numbers above about 10. The trend is similar to that observed in supernova remnants, but offset by about a factor of 3-4 in shock speed or 10 in Mach number, in the sense that the drop occurs at higher speeds in SNR shocks.

It is more difficult to determine electron and ion temperatures in shocks in the solar corona. Ma et al. (2011) observed a shock with AIA and used the ionization times of the Fe IX/X, Fe XII and Fe XIV that dominate several of the EUV bands to infer the electron temperature. The result suggested that $T_e/T_p \sim 0.25$. Also, UVCS

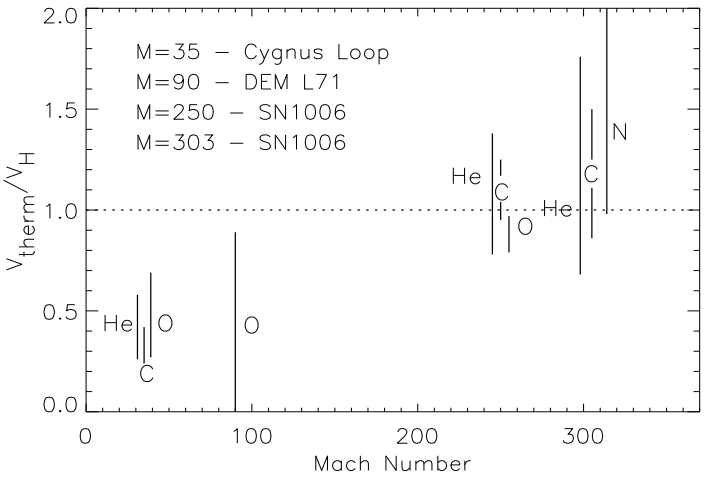

Figure 2: The ratios of the thermal velocities of He, C, N and O ions compared to those of hydrogen as a function of Mach number. The Cygnus Loop shock is close to thermal equilibrium, while both the SN1006 shocks are close to mass-proportional temperatures (Raymond et al. 2017).

spectra of coronal shocks generally show T_e/T_p or T_e/T_O less than one (Mancuso et al. 2002; Raouafi et al. 2004; Bemporad & Mancuso 2013; Bemporad, Susino & Lapenta 2014). The Mach numbers of these coronal shocks are modest, generally less than 2 or 3.

Although the electric field in the shock can play a role, efficient transfer of heat from protons to electrons requires some variety of plasma turbulence. Such turbulence can be effectively produced by two-stream instabilities between incident protons and protons reflected from the shock. The difficulty is that few wave modes can interact resonantly with both protons and electrons. Cargill & Papadopoulos (1988) proposed a two step process involving the Buneman and ion acoustic instabilities to heat the electrons to about 20% of the proton temperature. Lower-hybrid waves are able to interact with both protons and electrons, and Rakowski et al. (2008) show that LH waves in a cosmic ray-driven precursor could explain the observed decline of T_e/T_p with shock speed in SNRs.

5. ION-ION EQUILIBRATION

The temperatures of different ion species in SNR shocks can be measured from their line widths, which generally requires the observation of UV lines for comparison with the H I Balmer lines. Even modest reddening makes the UV lines too faint to observe. To date only the non-radiative shocks in the Cygnus Loop, DEM L71 in the LMC, and SN1006 have been observed (Raymond et al. 2015; Ghavamian et al. 2007; Korreck et al. 2004; Raymond et al. 1995, 2017). Figure 2 shows the thermal line widths of lines

of He, C, N and O compared with the thermal width of hydrogen. The lowest Mach number shock, the one in the Cygnus Loop, shows thermal speeds consistent with $m_{\rm i}^{-1/2}$, which is to say that the temperatures are equal. The fastest shocks are those in SN1006, where all the velocities are consistent with the same value, meaning that $T_{\rm i} \propto m_{\rm i}$. In other words, there seems to be no exchange of energy among the different particle species in fast shocks, so the kinetic energy of each species is thermalized independently. The observational constraints are not extremely tight, however.

Only a few measurements are available for solar wind shocks. Berdichevsky et al. (1997) and Korreck et al. (2007) found that ions of He, C, O and Fe are preferentially heated in interplanetary shocks, that is the temperatures are more than mass-proportional. The heating depends on the upstream plasma β, the mass-to-charge ratio M/Q, and the angle between the shock and the magnetic field, but there is considerable scatter.

Ion-ion equilibration has received less theoretical attention than electron-ion equilibration because it is less crucial for diagnostic applications, though the post-shock proton temperature depends significantly on whether He and H equilibrate. Fuselier & Schmidt (1994) studied preferential heating of higher M/Q ions, whose larger gyroradii cause them to experience a larger potential change in the electric field of the shock. Zimbardo (2011) studied the reflection of heavy ions at a shock, finding that the reflected ions reached more than mass-proportional temperatures and that the distributions are highly asymmetric in the sense that $T_\perp > T_\parallel$.

6. PARTICLE ACCELERATION

Particle acceleration is one of the most important processes in collisionless shocks. The central questions are what fraction of the energy dissipated by a shock goes into energetic particles and how it is distributed among the particle species. The latter focuses on electrons vs. protons, but elemental abundance anomalies offer clues to the acceleration process and the location of the accelerating shocks.

One approach is to determine the shock speed from a proper motion and distance, then compare the thermal energy predicted by the jump conditions with the measured proton and electron temperatures. Salvesen et al. (2009) and Medina et al. (2014) applied this method to ∼350 km/s shocks in the Cygnus Loop and found that in some cases there was not even enough energy to account for the electron and proton temperatures, probably due to an underestimate of the distance. Hovey et al. (2017) studied two Balmer line SNRs in the LMC, taking advantage of the reliably known distance. They obtained upper limits of 7% of the energy of 1800 - 4000 km/s shocks going into non-thermal particles.

In both the Cygnus Loop and LMC SNR cases, the proton temperature was determined from the Hα profiles in Balmer line shocks, and it is expected that neutrals in the pre-shock gas will damp the plasma turbulence needed to scatter energetic particles. Also, neutrals formed by charge exchange can pass back through the shock, depositing energy and momentum upstream. These processes can limit the maximum particle energy, reduce the efficiency of CR acceleration and steepen the spectrum (e.g. Drury, Duffy & Kirk 1996; Ohira 2012; Morlino & Blasi 2016). The presence of neutrals can also provide fast particles for injection into the DSA process (Ohira 2106). The acceleration efficiency also depends on the Mach number (Blasi et al. 2005; Vink et al. 2010)

A key part of DSA theory is the turbulent precursor where particles are scattered back toward the shock jump. Heating in the precursor broadens the narrow component of the Hα line beyond the normal width of the ISM line (Hester et al. 1994; Sollerman et al. 2003; Medina et al. 2014), but the interpretation is complicated by heating due to neutrals that cross into the precursor from the downstream region (Morlino et al. 2012). The thickness of the precursor tends to be around $1''$, and it has been spatially resolved in Tycho's SNR (Lee et al. 2007) and the Cygnus Loop (Katsuda et al. 2016).

As far as shocks in the heliosphere, Giacalone (2012) found that essentially all interplanetary shocks with Alfvén Mach numbers above 3 produce energetic particles whose spectrum is consistent with the diffusive shock acceleration picture. Mewaldt et al. (2005) found that fast CMEs put about 10% of their energy into SEPs.

The composition of CRs and SEPs can show the effects of the Q/M depedendence of diffusive shock acceleration, but in the case of heliospheric shocks there are large variations in ratios such as Fe/O and in the abundance of ^{3}He. This is attributed to more efficient injection of suprathermal particles into the diffusive acceleration process and differences in the populations of these suprathermals in the solar wind (e.g. Tylka & Lee 2006).

7. NON-MAXWELLIAN VELOCITY DISTRIBUTIONS

Any velocity distribution containing a thermal core and a power law cosmic ray tail is non-Maxwellian by definition, but it is interesting to ask whether the core itself is Maxwellian. This is a difficult observational question because the observable emission lines are generally faint, and the Hα profiles consist of at least two components. Raymond et al. (2010) obtained a very deep spectrum of a shock in Tycho's SNR, and found that the broad component could not be fit with a Gaussian. Raymond et al. (2017) found a similar departure from Gaussian in a 3000 km/s shock in SN1006.

There are at least 5 explanations for these observations. There could simply be two or more shocks with different speeds within the spectrograph field of view. The shock could have a precursor strong enough to heat some neutrals to a substantial fraction of the post-shock temperature (Ohira 2014, Raymond et al. 2011). The neutrals that pass through the shock will become pickup ions, which have a non-Gaussian velocity distribution (Raymond et al. 2008). The beginning of a power law tail may affect the wings of the line. Or, finally, the velocity dependence of the charge transfer cross section produces an intrinsically non-Maxwellian profile in very fast shocks (Morlino et al. 2013). Kropotina et al. (2016) computed the relaxation of heavy ions in a shock in SNR ejecta, and the theory and observations are reviewed by Bykov et al. (2013).

8. MAGNETIC FIELD AMPLIFICATION

There is strong evidence for amplification of the magnetic field in the faster SNR shocks from the thickness of the X-ray synchrotron filaments (Vink & Laming 2003; Bamba et al. 2005). Post-shock fields above 100 μG are inferred, which is far more than expected from simple compression of the pre-shock interstellar field. The amplification is believed to result from currents generated by the streaming of cosmic rays in the precursor (Bell 2004). The mechanism may also be involved in density

inhomogenties (Rakowski et al. 2011; Ohira 2016) and stripes of non-thermal X-ray emission in Tycho's SNR (Eriksen et al. 2011; Bykov et al. 2011). Another mechanism for amplifying magnetic fields is the vorticity associated with density inhomogeneities overtaken by the shock (Giacalone & Jokipii 2007).

9. SUMMARY

The physics of collisionless shock waves is important for understanding structures in the ISM and in the heliosphere. The lack of thermal equilibrium, the amplification of magnetic fields and the acceleration of energetic particles play important roles in the evolution of explosive events and in the interpretation of observations. These phenomena are understood qualitatively, but a more quantitative understanding is needed.

Acknowledgment

This work was supported by Guest Observer Grants HST-GO-13436.01-A and HST-GO-14228.001-A from the Space Telescope Science Institute.

References

Bamba, A., Yamazaki, R., Yoshida, T., Terasawa, T. & Koyama, K.: 2005, *ApJ*, **621**, 793.
Bell, A. R.: 2004, *MNRAS*, **353**, 550.
Bemporad, A. & Mancuso, S.: 2013, *JAdR*, **4**, 287.
Bemporad, A., Susino, R. & Lapenta, G.: 2014, *ApJ*, **784**, 102.
Berdichevsky, D., Geiss, J., Gloeckler, G. & Mall, U.: 1997, *JGR*, **102**, 2623.
Blandford, R. & Eichler, D.: 1987, *Phys. Reports*, **154**, 1.
Blasi, P., Gabici, S. & Vannoni, G.: 2005, *MNRAS*, **361**, 907.
Bykov, A. M., Ellison, D. C., Osipov, S. M., Pavlov, G. G. & Uvarov, Yu. A.: 2011, *ApJL*, **735**, 40.
Bykov, A. M., Malkov, M. A., Raymond, J. C., Krassilchtchikov, A. M. & Vladimirov, A. E.: 2013, *SSRv*, **178**, 599.
Caprioli, D. & Spitkovsky, A.: 2014, *ApJ*, **794**, 47.
Cargill, P. J. & Papadopoulos, K.: 1988, *ApJL*, **329**, L29.
Chevalier, R. A. & Raymond, J. C.: 1978, *ApJL*, **225**, L27.
Chevalier, R. A., Kirshner, R. P. & Raymond, J. C.: 1980, *ApJ*, **235**, 186.
Draine, B. T. & McKee, C. F.: 1993, *Ann. Revs. AA*, **31**, 373.
Drury, L. O'C., Duffy, P. & Kirk, J. G.: 1996, *A&A*, **309**, 1002.
Ellison, D. Baring, M. G. & Jones, F. C.: 1996, *ApJ*, **473**, 1029.
Eriksen, K. A. et al.: 2011, *ApJL*, **728**, 28.
Fermi, E.: 1949, *PhRv*, **75**, 1169.
Fuselier, S. A. & Schmidt, W. K. H.: 1994, *JGR*, **99**, 11539.
Ghavamian, P., Raymond, J. C., Smith, R. C. & Hartigan, P.: 2001, *ApJ*, **547**, 995.
Ghavamian, P., Winkler, P. F., Raymond, J. C. & Long, K. S.: 2002, *ApJ*, **572**, 888.
Ghavamian, P., Blair, W. P., Sankrit, R., Raymond, J. C. & Hughes, J. P.: 2007, *ApJ*, **664**, 304.
Ghavamian, P., Schwartz, S. J., Mitchell, J., Masters, A. & Laming, J. M.: 2013, *SSRv*, **178**, 633.
Giacalone, J.: 2012, *ApJ*, **761**, 28.
Giacalone, J.: 2015, *ApJ*, **848**, 123.
Giacalone, J. & Jokipii, J. R.: 2007, *ApJL*, **663**, 41.
Gopalswamy, N. & Yashiro, S.: 2011, *ApJL*, **736**, L17.
Gopalswamy, N., Nitta, N., Akiyama, S., Mäkalä, P. & Yashiro, S.: 2012, *ApJ*, **744**, 72.

Hester, J. J., Raymond. J. C. & Blair, W. P.: 1994, *ApJ*, **420**, 721.
Hovey, L., Hughes, J. P., McCully, C., Pandya, V. & Eriksen, K.: 2017, astro-ph 1709.08273.
Katsuda, S. et al.: 2016, *ApJL*, **819**, L32.
Korreck, K. E., Raymond, J. C., Zurbuchen, T. H. & Ghavamian, P.: 2004, *ApJ*, **615**, 280.
Korreck, K. E., Zurbuchen, T. H., Lepri, S. T. & Raines, J. M.: 2007, *ApJ*, **659**, 773.
Kropotinia, Yu. A., Bykov, A. M., Krassil'shchikov, A. M. & Levenfish, K. P.: 2016, *JTePh*, **61**, 517.
Lee, J.-J. et al.: 2007, *ApJL*, **659**, L133.
Long, K. S., Reynolds, S. P., Raymond, J. C., Winkler, P. F., Dyer, K. K. & Petre, R.: 2003, *ApJ*, **586**, 1162.
Ma, S. et al.: 2011, *ApJ*, **738**, 160.
Mancuso, S., Raymond, J. C., Kohl, J., Ko, Y.-K., Uzzo, M. & Wu, R.: 2002, *A&A*, **383**, 267.
Mancuso, S., Raymond, J. C., Kohl, J., Ko, Y.-K., Uzzo, M. & Wu, R.: 2003, *A&A*, **400**, 347.
Medina, A., Raymond, J. C., Edgar, R. E., Caldwell, N., Fesen, R. A. & Milisavljevic, D.: 2014, *ApJ*, **791**, 30.
Mewaldt, R. A. et al.: 2005, *ICRC*, **1**, 129.
Morlino, G. & Blasi, P.: 2016, *A&A*, **589**, A7.
Morlino, G., Bandiera, R., Blasi, P. & Amato, E.: 2012, *ApJ*, **760**, 137.
Morlino, G., Blasi, P., Bandiera, R. & Amato, E.: 2013, *A&A*, **558**, 25.
Ohira, Y.: 2012, *ApJ*, **758**, 97.
Ohira, Y.: 2014, *MNRAS*, **440**, 514.
Ohira, Y.: 2016, *ApJ*, **817**, 137.
Oka, M. et al.: 2017, *ApJ*, **842**, L11.
Ontiveros, V. & Vourlidas, A.: 2009, *ApJ*, **693**, 267.
Pick, M. & Vilmer, N.: 2008, *A&A Suppl.*, **16**, 1.
Rakowski, C. E., Laming, J. M. & Ghavamian, P.: 2008, *ApJ*, **684**, 348.
Rakowski, C. E., Laming, J. M., Hwang, U., Eriksen, K. A., Ghavamian, P. & Hughes, J. P.: 2011, *ApJL*, **735**, L21.
Raouafi, N. E. et al.: 2004, *A&A*, **424**, 1039.
Raymond, J. C., Blair, W. P. & Long, K. S.: 1995, *ApJL*, **454**, L34.
Raymond, J. C. et al.: 2000, *GRL*, **27**, 1439.
Raymond, J. C., Isenberg, P. A. & Laming, J. M.: 2008, *ApJ*, **682**, 408.
Raymond, J. C., Winkler, P. F., Blair, W. P., Lee, J.-J. & Park, S.: 2010, *ApJ*, **712**, 901.
Raymond, J. C., Vink, J., Helder, E. A. & de Laat, A.: 2011, *ApJL*, **731**, L14.
Raymond, J. C., Edgar, R. J., Ghavamian, P. & Blair, W. P.: 2015, *ApJ*, **805**, 152.
Raymond, J. C., Winkler, P. F., Blair, W. P. & Laming, J. M.: 2017, *ApJ*, in press.
Salvesen, G., Raymond, J. C. & Edgar, R. J.: 2009, *ApJ*, **702**, 327.
Schwartz, S. J., Thomsen, M. F., Bame, S. J. & Stansberry, J.: 1988, *JGR*, **93**, 12923.
Sironi, L. & Spitkovsky, A.: 2011, *ApJ*, **726**, 75.
Slane, P. et al.: 2014, *ApJ*, **783**, 33.
Sollerman, J., Ghavamian, P., Lundqvist, P. & Smith, R. C.: 2003, *A&A*, **407**, 249.
Susino, R., Bemporad, A. & Mancuso, S.: 2015, *ApJ*, **812**, 119.
Treumann, R. A.: 2009, *A&ARv*, **17**, 409.
Tylka, A. J. & Lee, M. A.: 2006, *ApJ*, **646**, 1319.
Vink, J. & Laming, J. M.: 2003, *ApJ*, **584**, 758.
Vink, J. S., Yamazaki, R., Helder, E. A. & Schure, K. M.: 2010, *A&A*, **722**, 131.
Vršnak, B., Magdalenić, J., Aurass, H. & Mann, G.: 2002, *A&A*, **396**, 673.
Zimbardo, G.: 2011, *P&SS*, **59**, 468.